Constraining gluon density of pions at large x by pion-induced J/ψ production

Wen-Chen Chang

Institute of Physics, Academia Sinica, Taipei 11529, Taiwan

Jen-Chieh Peng

Department of Physics, University of Illinois at Urbana-Champaign, Urbana, Illinois 61801, USA

Stephane Platchkov

IRFU, CEA, Université Paris-Saclay, 91191 Gif-sur-Yvette, France

Takahiro Sawada

Department of Physics, Osaka City University, Osaka 558-8585, Japan

Abstract

The gluon distributions of the pion obtained from various global fits exhibit large variations among them. Within the framework of the color evaporation model, we show that the existing pion-induced J/ψ production data, usually not included in the global fits, can impose useful additional constraints on the pion parton distribution functions (PDFs). In particular, these data can probe the pion's gluon densities at large x. Existing pion-induced J/ψ data covering a broad range of beam momenta are compared with next-to-leading-order QCD calculations using various sets of pion PDFs. It is found that J/ψ data measured at forward rapidity and at sufficiently high beam momentum are sensitive to the large-x gluon distribution of pions. The current J/ψ data favor the Sutton-Martin-Roberts-Stirling and Gluck-Reya-Vogt pion PDFs, containing significant gluon content at large x.

I. INTRODUCTION

The pion, as the Goldstone boson of dynamical chiral symmetry breaking of the strong interaction, is the lightest QCD bound state. Because of its light mass, the pion plays a dominant role in the long-range nucleon-nucleon interaction [1]. Understanding the pion's internal structure is important to investigate the low-energy, nonperturbative aspects of QCD [2]. Even though the pion is theoretically simpler than the proton, its partonic structure is much less explored. As scattering off a pion target is not feasible, current knowledge on pion parton distribution functions (PDFs) mostly relies on the pion-induced Drell-Yan data. Since these fixed-target data are mostly sensitive to the valence-quark distributions at $x > 0.2$, the sea and gluon densities are essentially unconstrained.

In principle, the prompt-photon production process $\pi N \to \gamma X$ can constrain the gluon content of pions through the $Gq \to \gamma q$ subprocess, but the experimental uncertainties are large. Production of heavy quarkonia, like J/ψ and Υ(1S), with the pion beam has distinctive advantages: The cross sections are large and they can be readily detected via the dimuon decay channel. These datasets have been shown to be sensitive to both the quark and gluon distributions of the incident pion with model-dependent assumptions of quarkonia fragmentation [3, 4]. The interesting possibility of accessing the pion PDFs from leading neutron deep inelastic scattering (DIS) data has been considered with promising results [5, 6]. However, this method is subject to large systematic uncertainties, and further studies on the uncertainties of the pion splitting function and the off-shellness of virtual pion are required [7, 8]. To precisely determine the sea quark content of pions, there was a suggestion of performing the Drell-Yan measurement with π^+ and π^- beams on the isoscalar deuterium target [9], and such a measurement is planned in a future experiment [10].

Until a couple of years ago, knowledge of the pion PDFs was limited to global analyses carried out more than two decades ago: Owens (OW) [11], Aurenche-Baier-Fontannaz-Kienzle-Focacci-Werlen (ABFKW) [12], Sutton-Martin-Roberts-Stirling (SMRS) [13], and Gluck-Reya-Vogt (GRV) [14], and Gluck-Reya-Schienbein (GRS) [15]. These analyses were based mostly on pion-induced Drell-Yan, often on prompt-photon and in some cases on J/ψ production data. New analyses were performed only recently, using the same Drell-Yan data in Bourrely-Soffer (BS) [16] as well as both the Drell-Yan and direct-photon data in xFitter [17]. The analysis of JAM [18] included both the Drell-Yan data and, for the first time, the leading neutron tagged electroproduction data. The experimental situation is also evolving. After more than two decades,

a new measurement of pion-induced Drell-Yan production cross sections was performed by the CERN COMPASS Collaboration [19]. The data are expected to be available in the near future. A proposal dedicated to investigating the pion and kaon structure at the future electron-ion collider in the U.S. [20] was recently described in Ref. [21].

On the theoretical side, the interest in the meson structure has considerably increased in recent years. Numerous new calculations, based on the chiral-quark model [22–24], Nambu-Jona-Lasinio model [25], light-front Hamiltonian [26, 27], holographic QCD [28, 29], maximum entropy method [30], and continuum functional approach using Dyson-Schwinger equations (DSE) [31–36], became available. A major breakthrough in lattice QCD [37] led several groups to perform a direct calculation of the pion valence x distribution [38–42]. Further improvement in the accuracy of the lattice calculations is anticipated. As of today, most of the theoretical predictions deal with the pion valence-quark distribution only. The gluon and sea PDFs are predicted solely within the DSE continuum approach [36].

In this work we investigate the sensitivity of the J/ψ production data to the pion PDFs. The theoretical challenge of this reaction comes from the treatment of the hadronization of $c\bar{c}$ pairs into a charmonium bound state. This nonperturbative process has been modeled in several theoretical approaches including the color evaporation model (CEM) [43], the color-singlet model (CSM) [44], and nonrelativistic QCD (NRQCD) [45]. The CEM assumes a constant probability for $c\bar{c}$ pairs to hadronize into a given charmonium. In the CSM, the production of J/ψ is assumed to be through the color-singlet $c\bar{c}$ channel of the same quantum numbers as J/ψ. The NRQCD expands the calculations by the powers of the average velocity of $c\bar{c}$ pairs in the rest frame of J/ψ. The hadronization probability of each $c\bar{c}$ pair depends on its color and spin state. More details about these theoretical frameworks can be found in Ref. [46]. In general, the CSM and NRQCD provide a good description of data taken at collider energies but fail to explain measurements at fixed-target energies [47].

To explore the constraints on the pion PDFs by the J/ψ production process, a theoretical model with a minimal number of parameters is preferred. A great feature of the CEM is that it is essentially parameter-free, except for a single effective parameter that accounts for the probability of $c\bar{c}$ pairs to hadronize into a particular quarkonium bound state. In spite of its well-known limitations [48], the CEM gives a good account of many features of fixed-target J/ψ cross section data with proton beams, including their longitudinal momentum (x_F) distributions [49, 50] and the collider data at RHIC, Tevatron, and LHC [51, 52]. Since the proton PDFs are well known

from other processes (DIS, Drell-Yan, etc.), the proton-induced J/ψ data are useful for validating the CEM as a suitable model. In contrast, the pion-induced J/ψ data involve the poorly known pion's PDFs. Therefore, we use the CEM to study the sensitivity of available J/ψ production data to the pion PDFs, especially the gluon distributions.

In the fixed-target energy domain, where the transverse momentum of the charmonium is less than its mass, the charmonium production is dominated by the quark-antiquark ($q\bar{q}$) and gluon-gluon fusion (GG) partonic processes. The shape of the longitudinal momentum x_F cross section is, therefore, sensitive to the quark and gluon parton distributions of colliding hadrons. Since the nucleon PDFs are known with good accuracy, the measurement of the x_F distribution of J/ψ production with the pion beam provides, within the theoretical model uncertainties, valuable information about the pion quark and gluon partonic distributions. Our study is performed using next-to-leading-order (NLO) CEM calculation, including the recent nucleon PDFs. The available pion-induced J/ψ data on hydrogen and several light-mass nuclear targets are compared to calculations using the available pion PDFs. Over the broad energy range considered, all pion PDF sets provide reasonable agreement with the x_F-integrated cross sections. In contrast, for the x_F distributions, we find that the agreement between data and calculations strongly depends on the magnitude and shape of the pion gluon distribution.

This paper is organized as follows. In Sec. II, we briefly describe the CEM framework for the calculations of J/ψ production cross sections in the collisions of pions and nucleons. Some distinctive features of parton densities in various pion PDFs used for the calculations are presented in Sec. III. The NLO CEM calculations using various pion PDFs are compared with the existing J/ψ production data in Sec. IV. Section V shows the results of systematic study for the CEM calculation. We discuss our findings from the comparison of CEM calculations with data in Sec. VI, followed by a summary in Sec. VII.

II. COLOR EVAPORATION MODEL AND HEAVY-QUARK PAIR PRODUCTION

The theoretical treatment of heavy quarkonium production consists of the QCD description of the production of heavy-quark pairs ($Q\bar{Q}$) at the parton level, and their subsequent hadronization into the quarkonium states. One of the theoretical approaches is NRQCD [45], where the cross section of quarkonium production is expanded in terms of the strong coupling constant α_S and the $Q\bar{Q}$ velocity. The cross section is factorized into the hard and soft parts for each color and spin

state of the $Q\bar{Q}$ pairs. The short-distance hard part is calculated perturbatively as a series of α_S in perturbative QCD (pQCD). The soft part consists of long-distance matrix elements (LDMEs) characterizing the probability of hadronization process for each color and spin state. The LDMEs are determined by a fit to the experimental data. In the color-singlet model [44], the production channel is assumed to be the color-singlet $Q\bar{Q}$ state with quantum numbers exactly matching those of the heavy quarkonium.

Based on quark-hadron duality, the CEM assumes a constant probability for $Q\bar{Q}$ pairs to hadronize into a quarkonium state. Taking J/ψ as an example, one first produces a $c\bar{c}$ pair via various QCD hard processes. For $c\bar{c}$ with an invariant mass $M_{c\bar{c}}$ less than the $D\bar{D}$ threshold, a constant probability F, specific for each quarkonium, accounts for the hadronization of $c\bar{c}$ pairs into the colorless J/ψ state.

In the CEM, the differential cross section $d\sigma/dx_F$ for J/ψ from the πN collision is expressed as

$$\frac{d\sigma}{dx_F}|_{J/\psi} = F \sum_{i,j=q,\bar{q},G} \int_{2m_c}^{2m_D} dM_{c\bar{c}} \frac{2M_{c\bar{c}}}{s\sqrt{x_F^2 + 4{M_{c\bar{c}}}^2/s}}$$
$$\times f_i^{\pi}(x_1,\mu_F) f_j^{N}(x_2,\mu_F) \hat{\sigma}[ij \to c\bar{c}X](x_1 p_\pi, x_2 p_N, \mu_F, \mu_R), \tag{1}$$

$$x_F = 2p_L/\sqrt{s},\ x_{1,2} = \frac{\sqrt{x_F^2 + 4{M_{c\bar{c}}}^2/s} \pm x_F}{2} \tag{2}$$

where i and j denote the interacting partons (gluons, quarks and antiquarks) and m_c, m_D, and $M_{c\bar{c}}$ are the masses of the charm quark, D meson, and $c\bar{c}$ pair, respectively. The f^{π} and f^{N} are the corresponding pion and nucleon parton distribution functions, respectively, evaluated at the corresponding Bjorken-x, x_1 and x_2, at the factorization scale μ_F.

The short-distance differential cross section of heavy-quark pair production $\hat{\sigma}[ij \to c\bar{c}X]$ is calculable as a perturbation series in the strong coupling $\alpha_s(\mu_R)$ evaluated at the renormalization scale μ_R. The variable s is the square of the center-of-mass energy of the colliding π-N system, and p_L is the longitudinal momentum of detected dimuon pair in the center-of-mass frame of π-N. It is assumed that the momenta of J/ψ and $c\bar{c}$ are approximately the same.

As mentioned above, the hadronization factor F is assumed to be universal, independent of the kinematics and the spin state of $c\bar{c}$ and the production subprocess. Therefore a unique feature of the CEM calculation is that the relative weight of each subprocess in $d\sigma/dx_F$, is fixed solely by the convolution of partonic-level cross sections $\hat{\sigma}$ and associated parton density distributions

f^{π} and f^{N} and, in particular, is independent of the F factor. The F factor is to be determined as the normalization parameter in the fit to the experimental measurements. The assumption of a common F factor for different subprocesses greatly reduces the number of free parameters in the CEM.

The leading-order $[\mathcal{O}(\alpha_S^2)]$ calculations of hard QCD kernel $\hat{\sigma}[ij \to c\bar{c}X]$ include the quark-antiquark ($q\bar{q}$) and gluon-gluon fusion (GG) diagrams. Additional quark-gluon Compton scattering (Gq, $G\bar{q}$) and virtual gluon corrections enter the NLO $[\mathcal{O}(\alpha_S^3)]$ calculations. The contributing partonic subprocesses in the fixed-order LO and NLO calculations are listed explicitly below [53]:

$$\begin{aligned} q + \bar{q} &\to Q + \bar{Q}, \alpha_S^2, \alpha_S^3 \\ G + G &\to Q + \bar{Q}, \alpha_S^2, \alpha_S^3 \\ q + \bar{q} &\to Q + \bar{Q} + g, \quad \alpha_S^3 \\ G + G &\to Q + \bar{Q} + g, \quad \alpha_S^3 \\ G + q &\to Q + \bar{Q} + q, \quad \alpha_S^3 \\ G + \bar{q} &\to Q + \bar{Q} + \bar{q}, \quad \alpha_S^3. \end{aligned} \tag{3}$$

Inclusion of both real and virtual gluon emission diagrams is necessary for calculating the full $\mathcal{O}(\alpha_S^3)$ cross sections.

In this work, we utilize the theoretical framework of NLO calculation of the total cross sections for production of the heavy-quark pair, developed by Nason *et al.* [53–55]. This framework has been widely used in the calculation of heavy-quark production. For example, it has been adopted in the NLO calculation of the CEM for J/ψ production in hadronic collisions[49–51]. With a few parameters including the heavy-quark mass m_c and hadronization factor F, the CEM calculations adequately reproduced the fixed-target data with proton, antiproton and pion beams [49, 50], as well as the collider data [51, 52].

III. PION PDFS

Pion-induced Drell-Yan data are included in all global analyses for the determination of the pion PDFs. However, Drell-Yan data [56–59] constrain mainly the valence-quark distribution. Without additional observables, the sea and gluon distributions remain practically unknown. Their magnitude can be only inferred through the momentum sum rule and valence-quark sum rule. Different

approaches have been taken to access the gluon and sea quark distributions: (i) utilizing J/ψ production data in OW [11]; (ii) utilizing the direct-photon production data [60] in ABFKW [12], SMRS [13], GRV [14], and xFitter [17]; (iii) utilizing leading neutron DIS [61, 62] in JAM [18]. In addition, some pion PDFs are based on theoretical modeling. For example, GRS [15] utilized a constituent quark model to relate the gluon and antiquark density, and BS [16] assumed quantum statistical distributions for all parton species with an universal temperature. We note that the OW analysis was performed at LO, whereas a NLO fit was carried out for all other analyses. Uncertainty bands for the resulting parton density distributions are available for two most recent global fits, JAM and xFitter. It was recently shown that the soft-gluon threshold resummation correction modifies the extraction of valence-quark distribution and, particularly, its falloff toward $x = 1$ [63]. This correction has not been implemented in any of the pion global analyses yet and it should affect only the calculated shape at the highest x_F region.

Figure 1 compares the valence, sea, and gluon momentum distributions of the OW, ABFKW, SMRS, GRV, JAM and xFitter pion PDFs at the scale of J/ψ mass. For clarity, we also show their ratios to GRV. Within $x \sim$0.1–0.8, the valence-quark distributions of SMRS, JAM and xFitter are close to each other, whereas those of OW, ABFKW, and GRV are lower by 20%–30%. The sizable error bands of the sea distributions provided by JAM and xFitter clearly indicate that the pion sea remains poorly known. As for the gluon distributions, the early PDF sets of OW, ABFKW, SMRS, and GRV have relatively large densities for $x > 0.1$, at variance with the recent xFitter and JAM PDFs that lie significantly lower. The spread of the gluon distributions around $x = 0.5$ among these six PDFs is even larger than the uncertainties of xFitter and JAM PDFs.

Table I lists the momentum fractions of valence quarks ($\bar{u}_{val}$), sea quarks ($\bar{u}_{sea}$), and gluons (G) of negative pions estimated by various pion PDFs at Q^2= 9.6 GeV^2, following the definitions of $\bar{u}_{val}(x) = \bar{u}(x) - \bar{u}_{sea}(x)$, $d_{val}(x) = d(x) - d_{sea}(x)$, $\bar{u}_{val}(x) = d_{val}(x)$, and $\bar{u}_{sea}(x) = d_{sea}(x)$. The values for the valence quarks show differences of up to 15%–20% but are nearly equal for the two more recent PDFs, JAM and xFitter. The gluon first moments vary from 0.29 for xFitter to 0.51 for GRV. The low gluon value in xFitter is compensated by a much larger sea contribution.

IV. RESULTS OF NLO CEM CALCULATIONS

In this section, we explore the sensitivity of the NLO CEM calculations to the various global fit parametrizations of the pion PDFs. We select four of them, namely, SMRS and GRV, as the

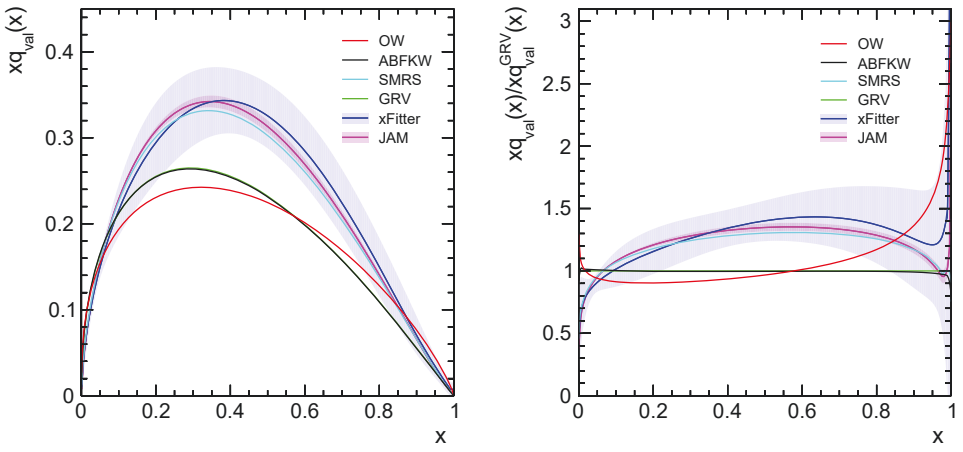

(a)

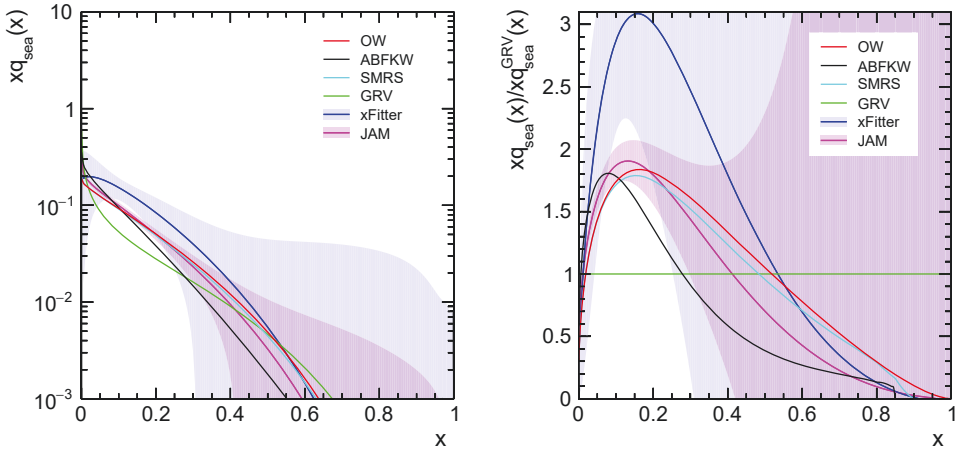

(b)

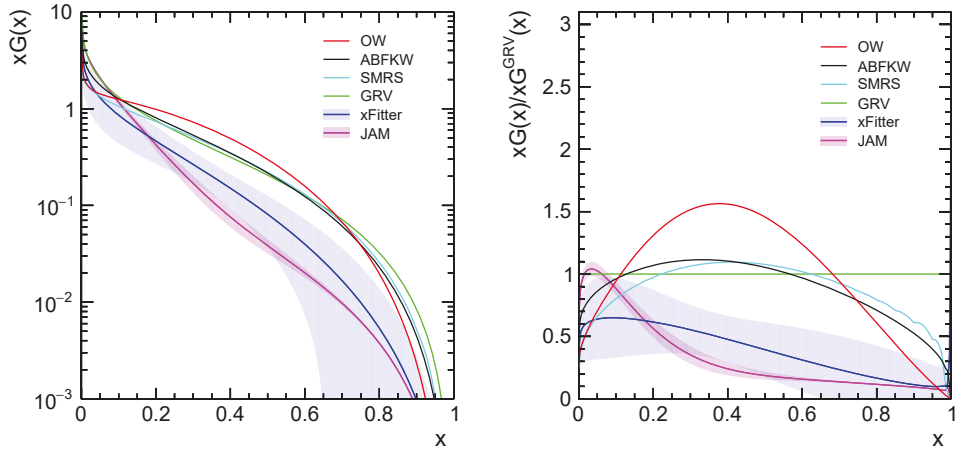

(c)

FIG. 1. Momentum density distributions $[xf(x)]$ of (a) valence quarks, (b) sea quarks, and (c) gluons of various pion PDFs and their ratios to GRV, at the scale of J/ψ mass (Q^2= 9.6 GeV^2).

PDF	$\int_0^1 x\bar{u}_{val}(x)dx$	$\int_0^1 x\bar{u}_{sea}(x)dx$	$\int_0^1 xG(x)dx$
OW	0.203	0.026	0.487
ABFKW	0.205	0.026	0.468
SMRS	0.245	0.026	0.394
GRV	0.199	0.020	0.513
JAM[a]	0.225 ± 0.003	0.028 ± 0.002	0.365 ± 0.016
xFitter[a]	0.228 ± 0.009	0.040 ± 0.020	0.291 ± 0.119

TABLE I. Momentum fractions of valence quarks, sea quarks and gluons of various pion PDFs for π^- at the scale Q^2= 9.6 GeV^2.

[a]Uncertainties estimated from the member PDF sets.

most widely used for a long time, and the two most recent fits, xFitter and JAM. Out of the three possible parametrizations for SMRS, we choose the one in which the sea quarks carry 15% of the pion momentum at Q^2= 4 GeV^2. As illustrated in Fig. 1, SMRS, JAM, and xFitter have quite similar valence-quark distributions while the magnitude of the GRV distribution is lower, by up to 20%–30%. As for the gluon distributions, SMRS and GRV have similar shapes and magnitudes, while the magnitudes of xFitter and JAM are significantly smaller, by a factor of 2–4.

As a first step, we compare the NLO CEM cross sections integrated over $x_F > 0$ for the process $\pi^- N \to J/\psi X$ for each of the four pion PDFs with the available measurements as a function of the center-of-mass energy $\sqrt{s}$ of the reaction. The calculations are performed using the nucleon CT14nlo PDFs [64] under the LHAPDF framework [65, 66]. The cross sections are evaluated with a charm quark mass $m_c = 1.5$ GeV/c^2 and renormalization and factorization scales of $\mu_R = m_c$ and $\mu_F = 2m_c$, respectively [55]. The experimental cross sections are taken from the compilation of Ref. [46]. For the sake of completeness, the subsequent measurement from the WA92 experiment [67] is also included, after correcting it for the nuclear dependence. The hadronization factors F are assumed to be energy independent and are determined by the best fit to the data for the central values of each pion PDF. The uncertainties of xFitter and JAM PDFs are not taken into account here.

The results and the comparison with data are displayed in Fig. 2. The total cross sections for the four PDFs exhibit quite similar $\sqrt{s}$ dependencies, and all agree reasonably with the data. The differences between them are visible through the F factors, which vary from 0.05 to 0.09. As

a general feature, the $q\bar{q}$ contribution dominates at low energies, whereas the GG contribution becomes increasingly important with increasing $\sqrt{s}$. However, the relative fractions of $q\bar{q}$ and GG contributions as a function of $\sqrt{s}$ vary considerably, reflecting the differences between the corresponding parton distributions. For SMRS and GRV, the GG contribution starts to dominate the cross section beyond $\sqrt{s} = 13$ and $\sqrt{s} = 11$ GeV, respectively, while for xFitter and JAM the corresponding values are much higher: $\sqrt{s} = 19$ and 21 GeV, respectively.

In order to investigate further the effect led by different pion PDFs, we compare the longitudinal x_F distribution of the calculated pion-induced J/ψ production cross section with a selection of fixed-target data from Fermilab and CERN experiments. Among the datasets available for pion-induced J/ψ production [68–77], we choose the ones that have large-x_F coverage for either hydrogen or light nuclear targets (lithium and beryllium) in order to minimize the effects of the nuclear environment. The selected eight datasets are listed in Table II. The beam momenta of the datasets cover the range of 39.5–515 GeV/c, corresponding to $\sqrt{s}$ values ranging from 8.6 to 31.1 GeV. Some of the data listed in Table II involve nuclear targets. The target PDFs parametrizations are CT14nlo for the hydrogen target and EPPS16 [78] for the lithium and beryllium targets. Contrary to the integrated cross sections, we now allow energy dependence for the hadronization factor F which is to be fine-tuned for each dataset individually.

Within the CEM and heavy-quark pair production framework introduced in Sec. II, we performed the LO and NLO calculations of the differential cross sections as a function of x_F with the charm quark mass $m_c = 1.5$ GeV/c^2 and renormalization and factorization scales $\mu_R = m_c$ and $\mu_F = 2m_c$, respectively [55]. The comparison of results with the selected data is shown in Figs. 3-10. In Fig. 3, where the dataset has the largest beam momentum, both LO and NLO CEM results calculated with SMRS, GRV, xFitter, and JAM pion PDFs are shown, whereas only NLO results are shown in the other figures.

The hadronization factor F, as an overall normalization parameter, is determined by the best χ^2 fit to the x_F distributions of cross sections, shown as the black lines in Figs. 3–10. The experimental normalization uncertainties listed in Table II are not included in the error estimation, since they are correlated systematic errors and will not affect the χ^2 but only contribute to the uncertainty of F factor. To compare the four pion PDFs on an equal footing, the uncertainties of the more recent PDFs are not included in the calculation of χ^2. We will discuss the impact of PDF uncertainties on the fit results later.

The χ^2/ndf value of the best fit is also displayed in the plot. The estimated individual $q\bar{q}$ and

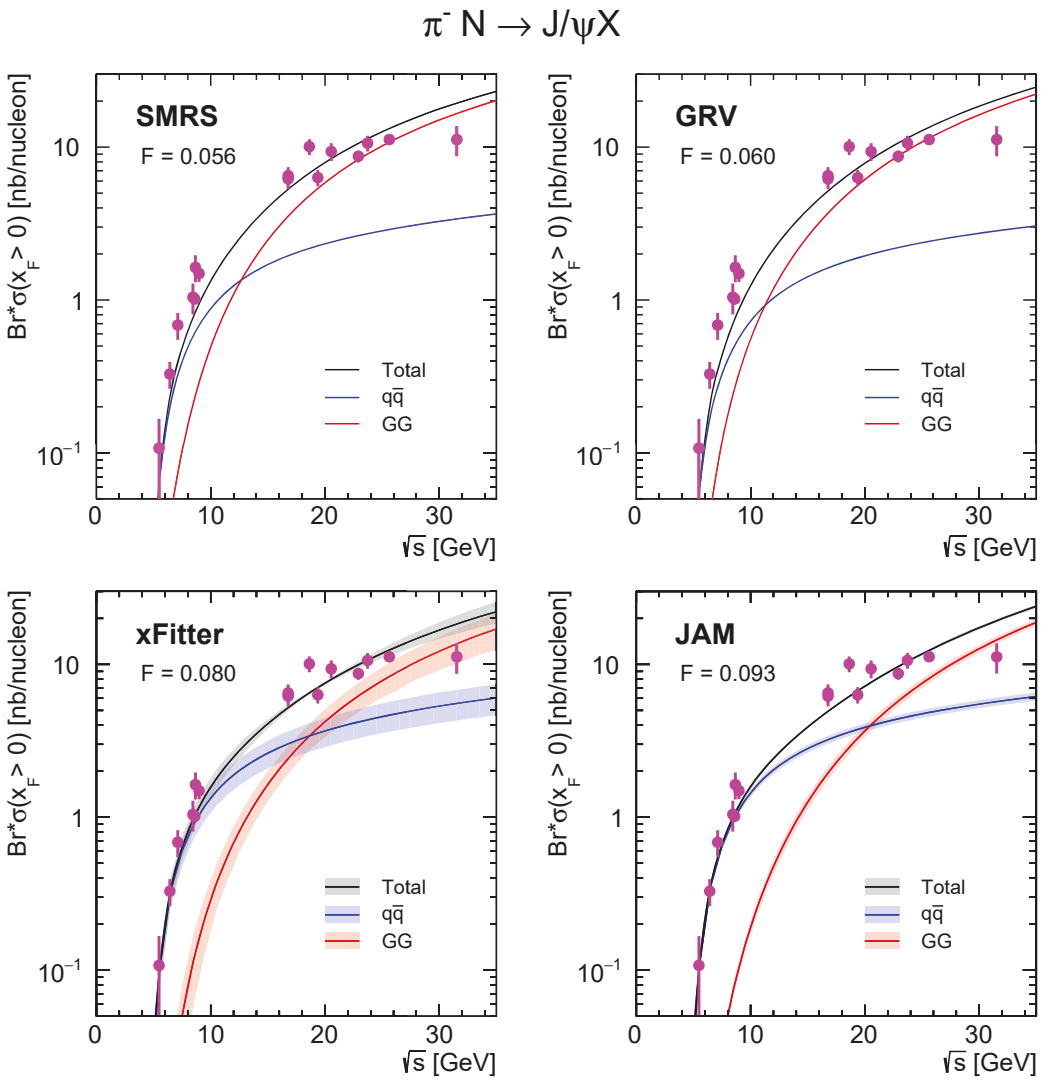

FIG. 2. The product of J/ψ dimuon decay branching ratio (Br) and J/ψ production cross sections at $x_F > 0$ for the $\pi^- N$ reaction, calculated with four pion PDFs (SMRS, GRV, xFitter and JAM) is compared with data (solid circles) [46, 67]. The black, blue, and red curves represent the calculated total cross section and the $q\bar{q}$ and GG contributions, respectively. The shaded bands on the xFitter and JAM calculations come from the uncertainties of the corresponding PDF sets. The SMRS and GRV PDFs contain no information on uncertainties.

GG contributions are denoted as blue and red lines, respectively. There is a negligible additional contribution from the qG subprocess, shown as green lines, to the total cross sections in the NLO calculation. The calculated value of the qG contribution is negative [53]. The uncertainties of xFitter and JAM PDF sets are displayed as shaded bands. In the following subsections (Secs. IV A–

Experiment	P_{beam} (GeV/c)	Target	Normalization[a]	References
FNAL E672, E706	515	Be	12.0	[68]
FNAL E705	300	Li	9.5	[69]
CERN NA3[b]	280	p	13.0	[70]
CERN NA3[b]	200	p	13.0	[70]
CERN WA11[b]	190	Be	[c]	[72]
CERN NA3[b]	150	p	13.0	[70]
FNAL E537	125	Be	6.0	[73]
CERN WA39[b]	39.5	p	15.0	[74]

TABLE II. The J/ψ production datasets with π^- beam used in the analysis, listed in order of decreasing beam momentum.

[a]Percentage of uncertainty in the cross section normalization.

[b]The numerical information was taken from figures.

[c]Information not available.

IV H), we briefly comment on the features of each experimental measurement and discuss the comparison of the data with the CEM calculations. Our observations are summarized in Sec. IV I.

A. Fermilab E672/E706 experiment

The Fermilab E672/E706 experiment [68] used a 515 GeV/c π^- beam scattered off 3.71- and 1.12-cm-long ^{9}Be targets. About 9600 J/ψ events integrated in the mass region between 2.8 and 3.4 GeV/c^2 were collected. The final cross sections cover the range $0.1 \leq x_F \leq 0.8$ in bins of 0.02 and have a normalization uncertainty of 12%.

The comparison of our calculations at both LO and NLO to the E672/E706 data is shown in Fig. 3. Judging from the reduced χ^2/ndf values, the NLO calculations with SMRS and GRV are in better agreement with the data than those with xFitter and JAM. The NLO calculation improves the description of the E672/E706 data only in the cases of SMRS and GRV. In comparison with the LO, the NLO calculation has a large effect on the cross sections, increasing its magnitude by more than a factor of 2. An interesting observation is that this increase in magnitude is nearly entirely compensated by the F factor, pointing to a nearly uniform increase along x_F. We also note that

the GG contribution dominates the cross section up to values of x_F as large as 0.5–0.7, depending on the particular pion PDF set. The additional qG term in the NLO calculation has a minor (and negative) contribution, although largely dependent on the particular PDF set.

We observe that the hadronization factor F is reduced by a factor of 4–5 from LO to NLO calculations. Since the NLO calculations involve higher-order QCD diagrams, the F factor, playing the role of a normalization constant of cross sections to describe the data, is expected to be different in the cases of LO and NLO calculations. An additional justification for the usage of NLO calculations comes from the fact that all four pion PDFs examined in this work are determined in a NLO global analysis.

B. Fermilab E705 experiment

The Fermilab E705 experiment [69] used a 300 GeV/c negative hadron beam (with 98% pions) scattered off a 33-cm-long lithium target. Data were also collected with a positive hadron beam consisting of protons and positive pions. Thanks to the open geometry spectrometer, an excellent mass resolution was achieved, allowing a measurement of the J/ψ peak in the mass range between 2.98 and 3.18 GeV/c^2. Since the final number of J/ψ events was not explicitly given, we estimate it from the published statistical errors to about 6000 events for the negative pion beam. The final cross sections have a normalization uncertainty of 11.1% and cover the range $-0.1 \leq x_F \leq 0.45$ in bins of 0.05.

The comparison of our calculations with the experimental cross sections is shown in Fig. 4. The best χ^2/ndf value is obtained with the SMRS PDFs. In contrast, the use of the JAM PDFs results in a significantly degraded χ^2/ndf. The GG contribution for the JAM PDFs has a falloff in x_F too fast to describe the data. We observe a trend similar to the one seen already in Fig. 3: The crossover between the central values of $q\bar{q}$ and GG terms for SMRS and GRV occurs at values of x_F much larger than the ones for xFitter and JAM.

C. CERN NA3 experiment, 280 GeV/c

The CERN NA3 experiment [70], performed nearly four decades ago, still has the largest pion-induced J/ψ production statistics available today. Data were taken at three different incident momenta, 280, 200, and 150 GeV/c with both positive and negative hadron beams. The beam

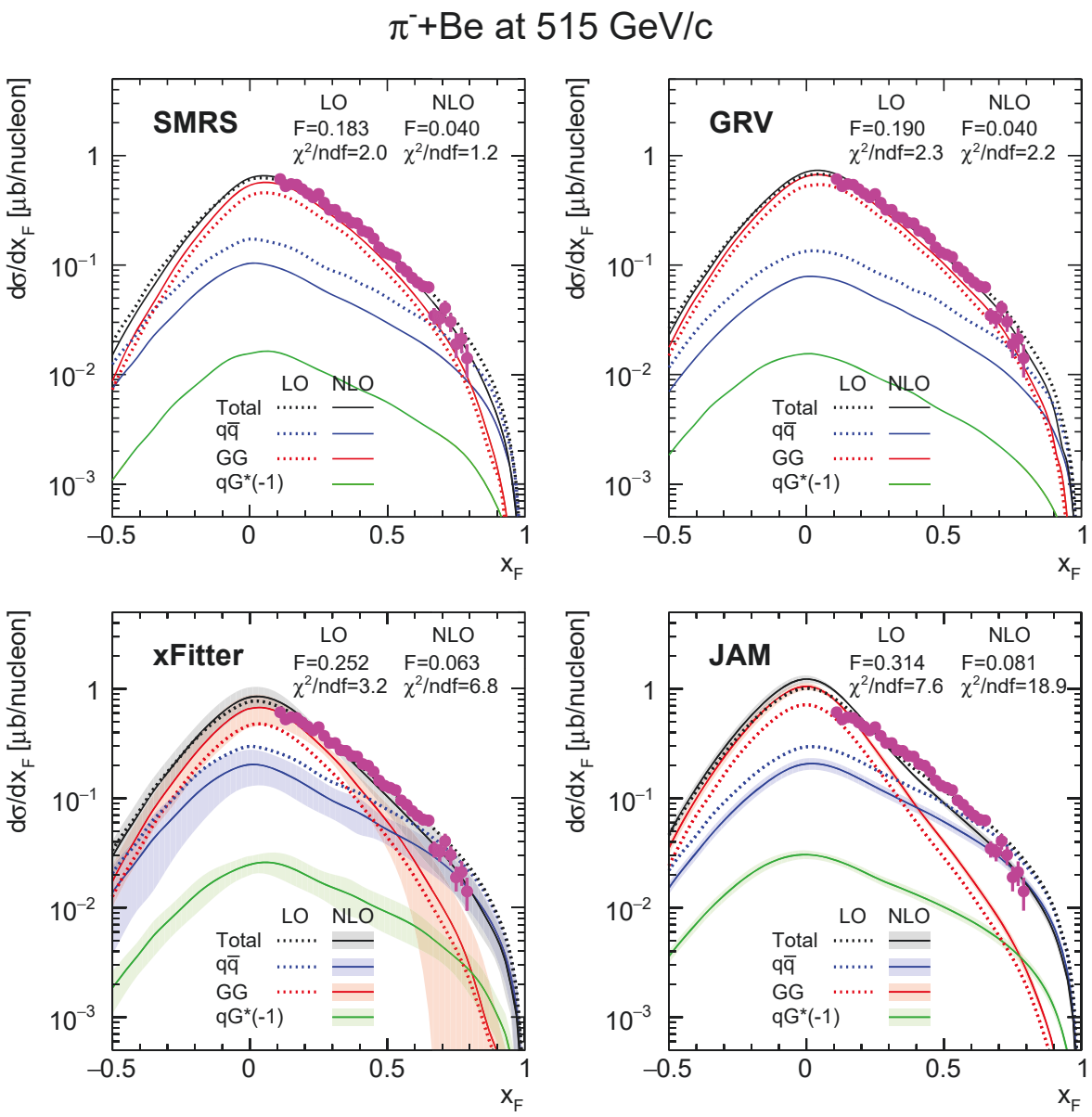

FIG. 3. Comparison of the LO and NLO CEM results for the SMRS, GRV, xFitter, and JAM PDFs, with the $d\sigma/dx_F$ data of J/ψ production off the beryllium target with a 515-GeV/c π^- beam from the E672/E706 experiment [68]. The total cross sections and $q\bar{q}$, GG, and $qG \times (-1)$ contributions are denoted as black, blue, red, and green lines, respectively. Solid and dotted lines are for the NLO and LO calculations, respectively. The shaded bands on the xFitter and JAM calculations come from the uncertainties of the corresponding PDF sets. For clarity, the resulting χ^2/ndf and F factors are also displayed.

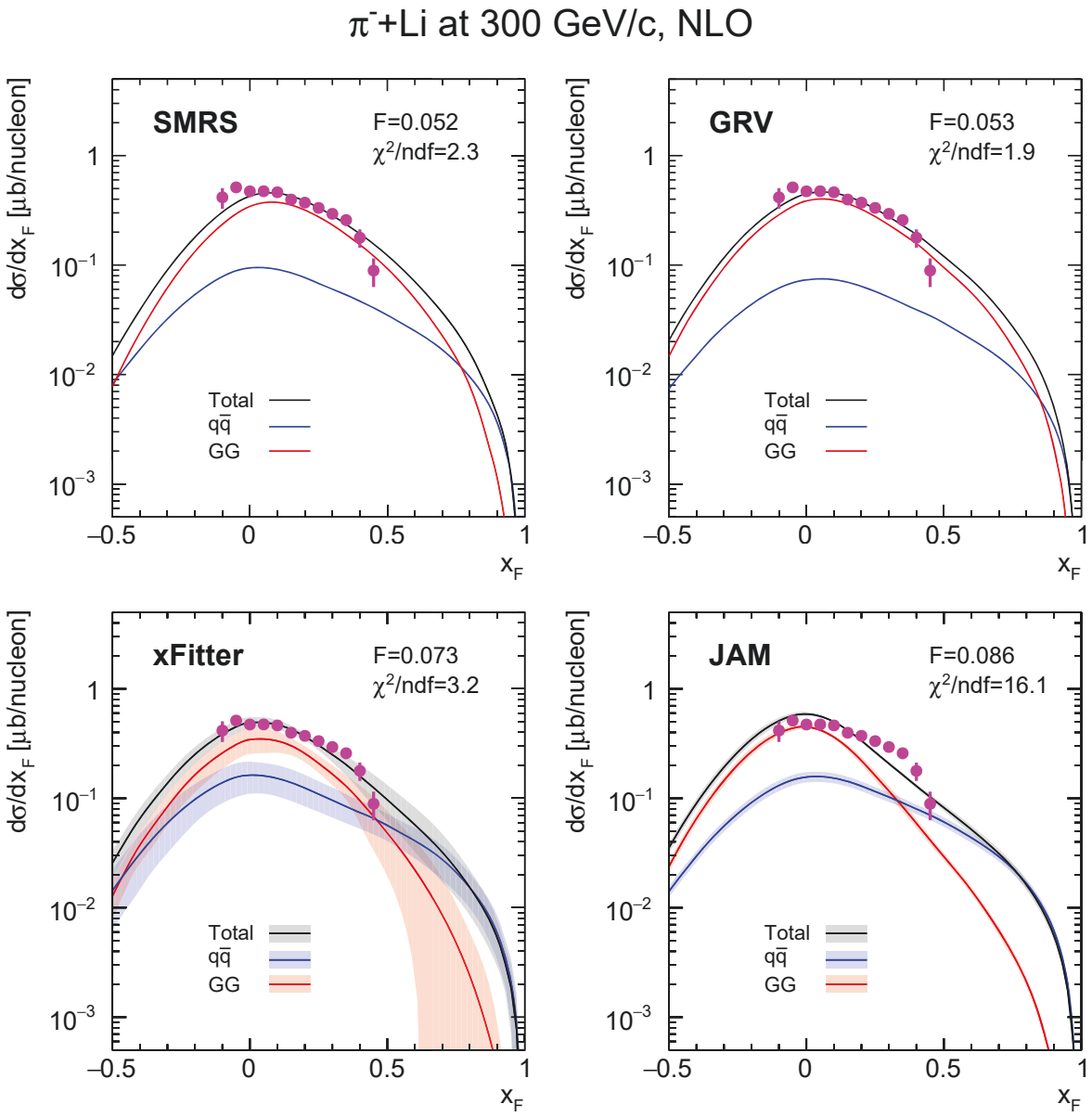

FIG. 4. Comparison of the NLO CEM results for the SMRS, GRV, xFitter, and JAM PDFs with $d\sigma/dx_F$ data of J/ψ production off the lithium target with a 300-GeV/c π^- beam from the E705 experiment [69]. The total cross sections and $q\bar{q}$ and GG contributions are denoted as black, blue, and red lines, respectively.

components were identified using Cherenkov counters. Moreover, in addition to a heavy platinum target, a liquid hydrogen target was also used, thus eliminating all possible nuclear effects. For all three energies, the cross sections have a normalization uncertainty of 13%. In the present study we consider only the NA3 hydrogen data. Unfortunately, these invaluable numerical cross sections were never published and could be retrieved only from the figures in the published paper [70] and

unpublished thesis [79].

For the 280 GeV/c data taking, the authors used a 50-cm-long hydrogen target, resulting in 23350 $J/\psi\ \pi^-$ events in the dimuon mass region between 2.7 and 3.5 GeV/c^2. The retrieved data are available in 17 x_F bins of 0.05, between 0.025 and 0.825. The comparison with the NLO CEM calculation is shown in Fig. 5. The resulting χ^2/ndf values repeat the trend already observed: They are better for the calculations with SMRS and GRV PDFs and are 2–4 times larger for xFitter and JAM. We note in passing that the relatively small χ^2/ndf values could partly be caused by the overestimation of the statistical errors in retrieving the original cross sections from the published figures.

D. CERN NA3 experiment, 200 GeV/c

The data at 200 GeV/c incident momentum were taken with a 30-cm-long hydrogen target. With the negative hadron beam 3157 pion-induced J/ψ events were collected. The retrieved data extend from $x_F = 0.05$ to $x_F = 0.85$.

The comparison of the NLO calculation with the data is shown in Fig. 6. The agreement with the data is fair for all PDF sets, although the general trend persists: The most recent xFitter and JAM global fits have slightly worse χ^2/ndf values. We also note that, as the incident momentum decreases, the importance of the $q\bar{q}$ term increases, particularly for the larger values of x_F. The GG contribution dominates the cross section for the calculation with the GRV PDFs up to $x_F = 0.6$. In contrast, for the JAM PDFs, the corresponding value is much lower: $x_F = 0.2$.

E. CERN WA11 experiment

The WA11 Collaboration at CERN measured J/ψ production cross sections [72] using a 190 GeV/c negative pion beam scattered off a triplet of beryllium target with a total length of 8.9 cm. Thanks to the open spectrometer geometry used, an excellent J/ψ mass resolution, $\sigma = 31$ MeV/c^2, was achieved. The large spectrometer coverage in dimuon opening angles made possible measurements at x_F values from –0.35 to 0.75, in bins of 0.10. About 38000 J/ψ events were reported in the mass range between 3.00 and 3.18 GeV/c^2, including 7% background. The same experiment had previously measured the feed-down contribution from the χ_c decays. In the cross sections shown, this contribution was subtracted. For consistency, the reported feed-down contri-

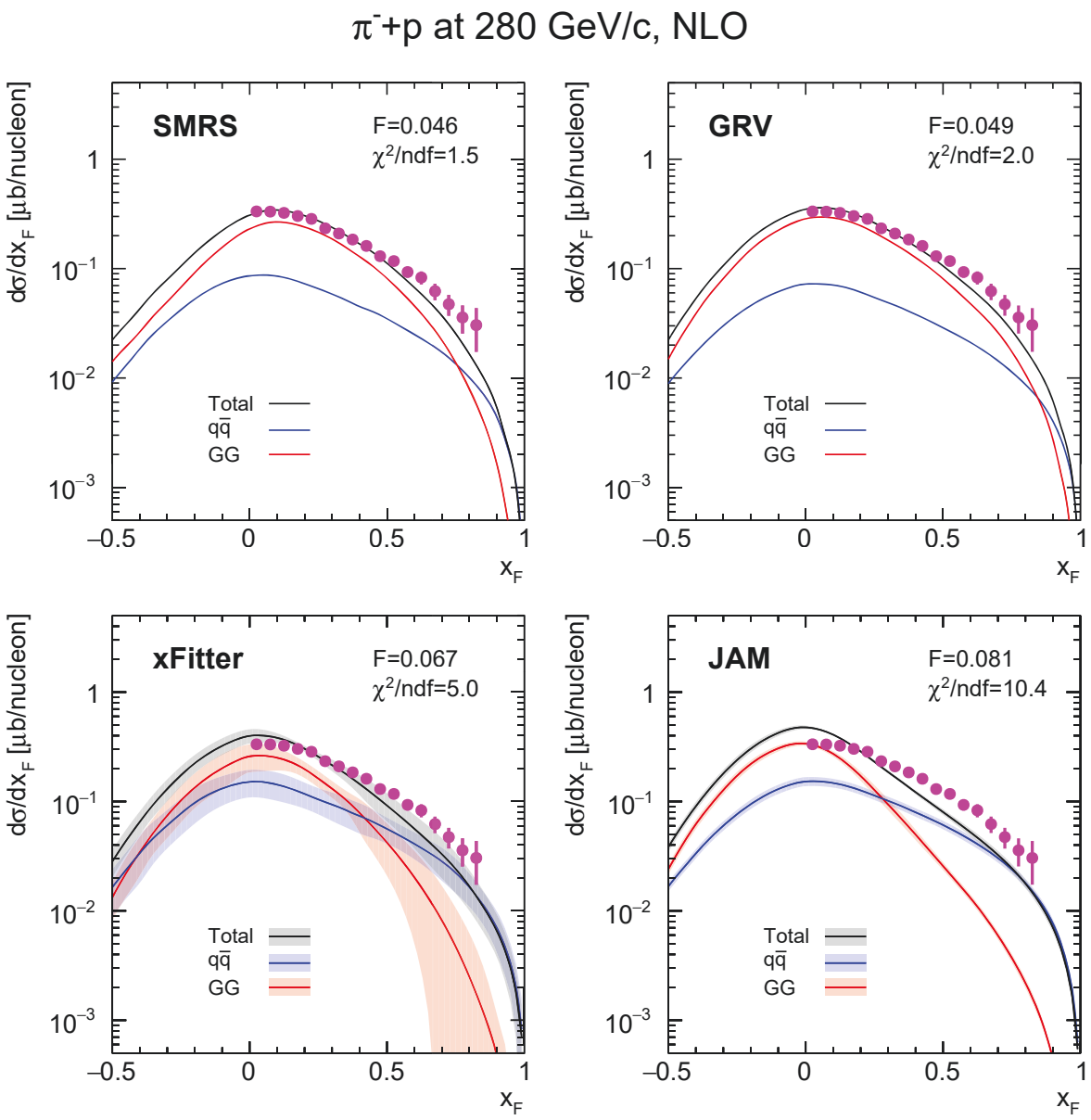

FIG. 5. Comparison of the NLO CEM results for the SMRS, GRV, xFitter and JAM PDFs, with the $d\sigma/dx_F$ data of J/ψ production off the hydrogen target with a 280-GeV/c π^- beam from the NA3 experiment [70]. The total cross sections and $q\bar{q}$ and GG contributions are denoted as black, blue, and red lines, respectively.

butions were added to the prompt cross section values shown, using the described procedure in reverse order.

The comparison of the NLO CEM calculations with the WA11 data is shown in Fig. 7. The resulting χ^2/ndf values are larger than for the NA3 data, pointing to additional systematic errors either in the original data or in the procedure of retrieving them. Not surprisingly, however, the

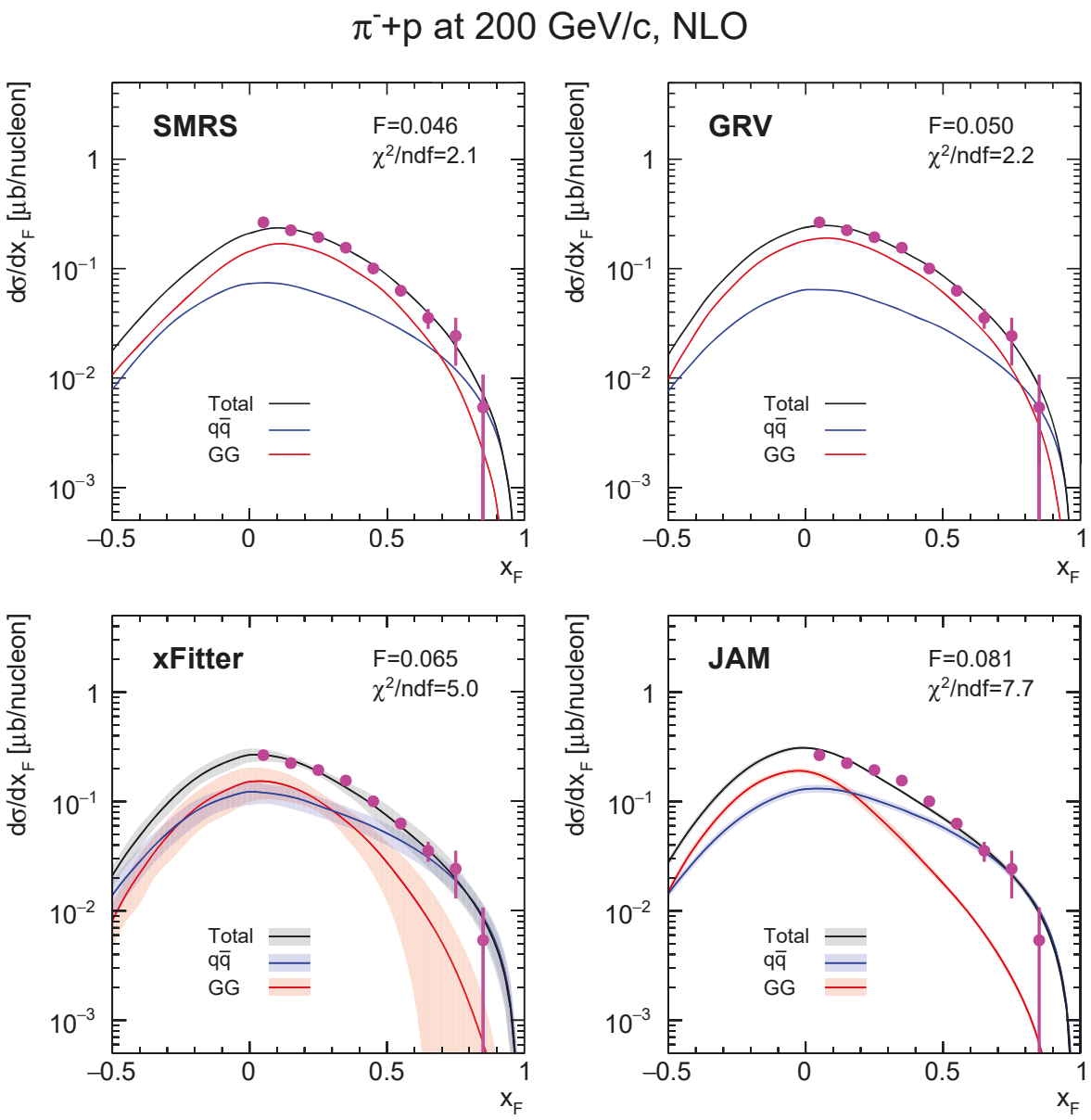

FIG. 6. Comparison of the NLO CEM results for the SMRS, GRV, xFitter, and JAM PDFs, with the $d\sigma/dx_F$ data of J/ψ production off the hydrogen target with a 200-GeV/c π^- beam from the NA3 experiment [70]. The total cross sections and $q\bar{q}$ and GG contributions are denoted as black, blue, and red lines, respectively.

overall conclusions are similar to the ones made previously for the 200 GeV/c data. The calculations with SMRS and GRV are in better agreement with the data than xFitter and JAM.

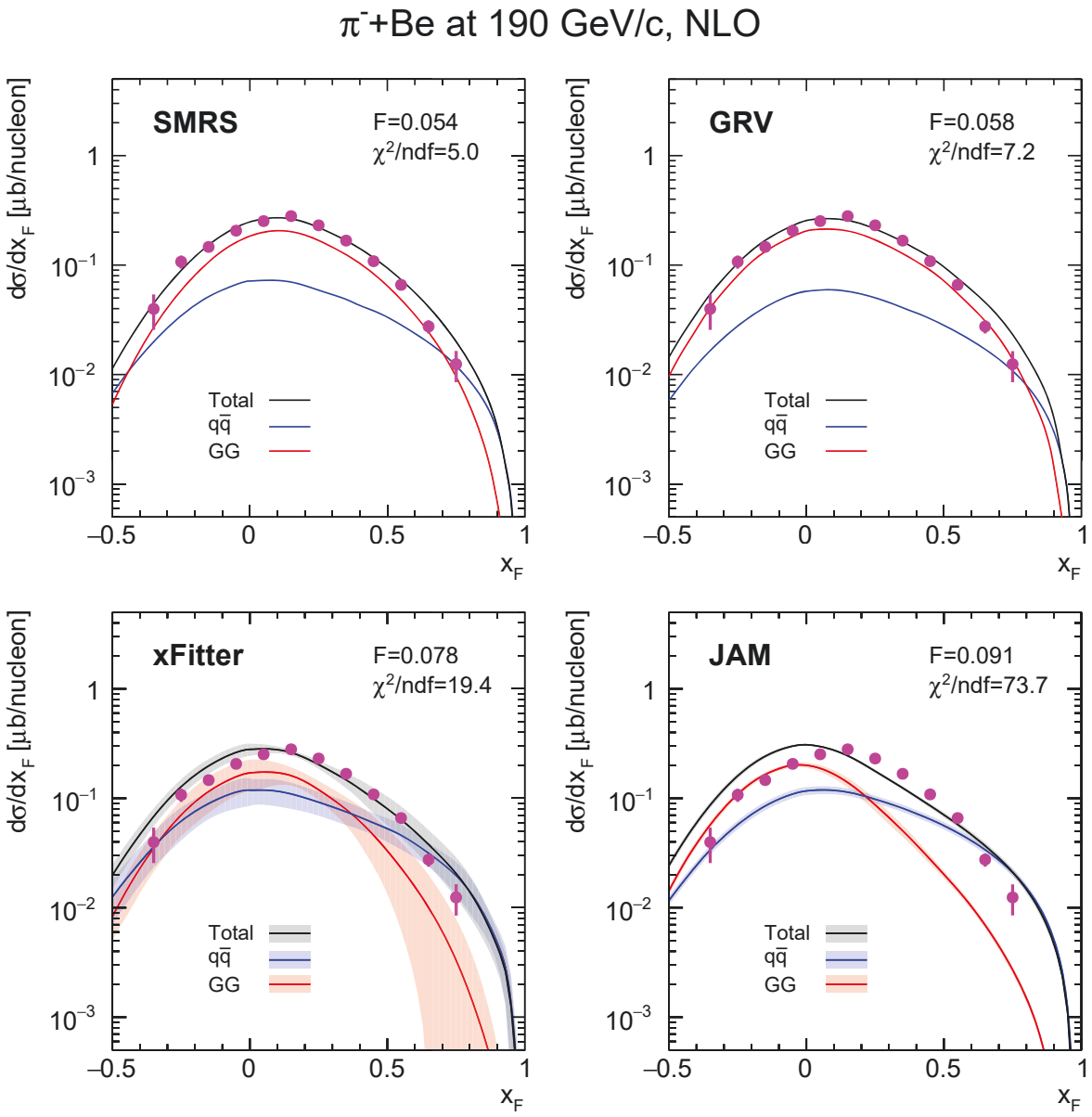

FIG. 7. Comparison of the NLO CEM results for the SMRS, GRV, xFitter, and JAM PDFs, with the $d\sigma/dx_F$ data of J/ψ production off the beryllium target with a 190-GeV/c π^- beam from the WA11 experiment [72]. The total cross sections and $q\bar{q}$ and GG contributions are denoted as black, blue, and red lines, respectively.

F. CERN NA3 experiment, 150 GeV/c

The NA3 data at 150 GeV/c were taken with a 30-cm-long hydrogen target. The statistics is large, as 16952 events were reported. The original data cover the x_F region between 0.025 and 0.975, in bins of 0.05. The data retrieved from the published figures extend to $x_F = 0.925$.

The comparison with the NLO CEM calculation is shown in Fig. 8. The calculated χ^2/ndf

values are rather small, pointing to somewhat overestimated experimental error bars. Nevertheless, they remain larger for the two most recent PDF sets. The overall trend previously observed is confirmed.

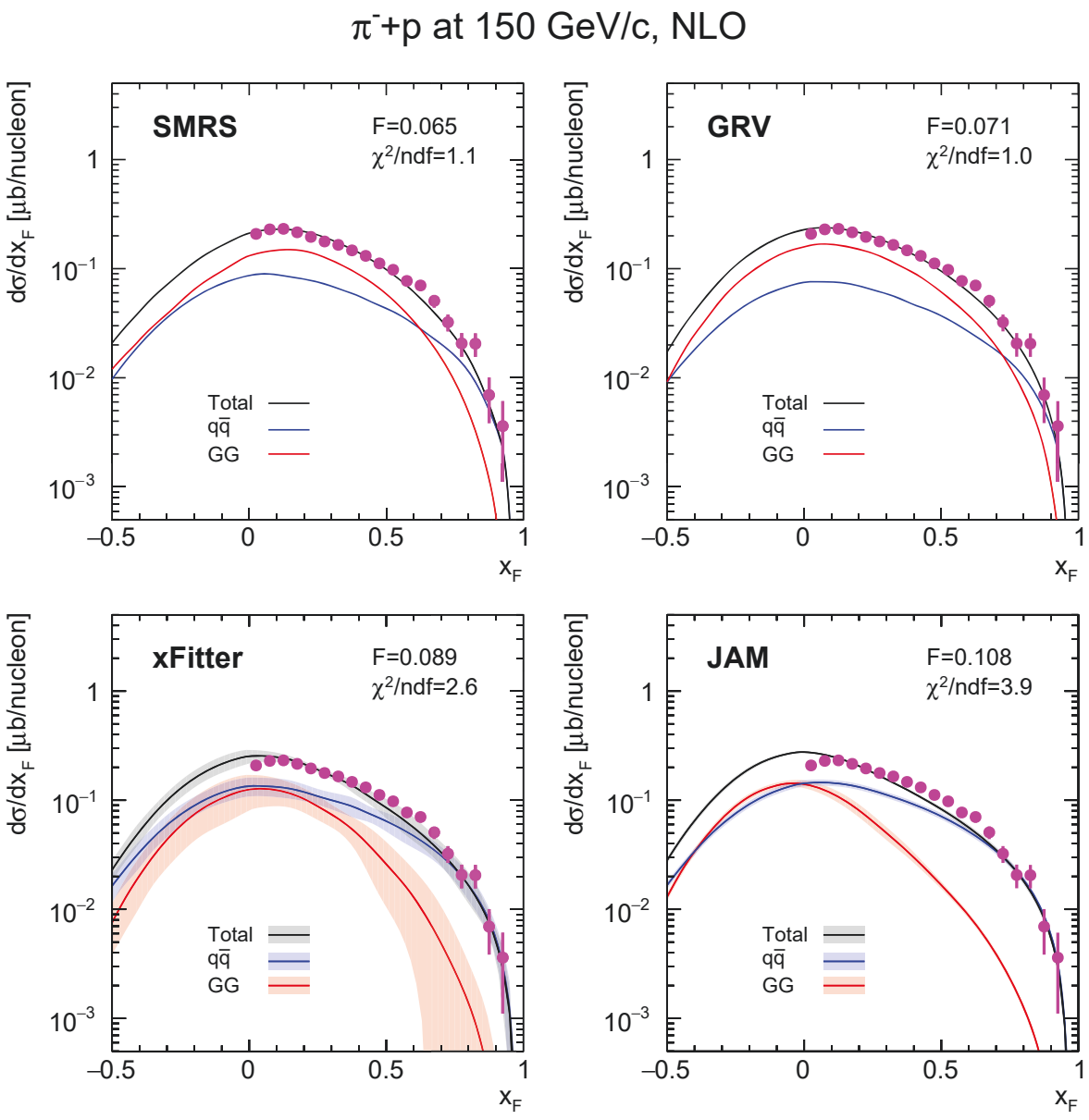

FIG. 8. Comparison of the NLO CEM results for the SMRS, GRV, xFitter and JAM PDFs, with the $d\sigma/dx_F$ data of J/ψ production off the hydrogen target with a 150-GeV/c π^- beam from the NA3 experiment [70]. The total cross sections and $q\bar{q}$ and GG contributions are denoted as black, blue, and red lines, respectively.

G. Fermilab E537 experiment

The E537 experiment at Fermilab has measured J/ψ production cross sections induced by a hadron beam of 125 GeV/c containing 82% negative pions and 18% antiprotons. Three different targets have been used: beryllium, copper, and tungsten. An experimental mass resolution of $\sigma = 200$ MeV/c^2 for the Be target is reported. The 2881 collected events with the Be target in the region of the J/ψ peak cover the x_F region between 0.05 and 0.95, in bins of 0.10. The normalization uncertainty on the cross sections is 6%.

The NLO CEM calculation and the E537 data are shown in Fig. 9. The χ^2/ndf values are reasonable for SMRS and GRV calculations and again slightly worse for xFitter and JAM. For values of $x_F \simeq 0$, the magnitude of the $q\bar{q}$ term is similar to that of the GG term. We also observe the relatively quick decrease of the GG term for the calculation with the JAM gluon PDF.

H. CERN WA39 experiment

The CERN WA39 Collaboration measured the J/ψ production cross section with a 39.5 GeV/c hadron beam momentum. Data for the 67-cm-long liquid hydrogen target were taken with negative and positive hadron beams. Measurements are reported with incident π^+, π^-, K^+, K^-, p and $\bar{p}$. Most of the 402 events reported for the negative hadron beam are pion-induced J/ψ's. The x_F-differential cross sections, available as a figure in the published paper, cover the region $0.05 \leq x_F \leq 0.85$ in bins of 0.10. The normalization uncertainty on the cross sections is 15%.

The comparison between data and calculations is shown in Fig. 10. The immediate observation is that for this low incident momentum the $q\bar{q}$ contribution is much larger than the GG term, by a factor of 5–8 around $x_F = 0$. The χ^2/ndf values for the four PDFs are all close to 1 and slightly larger for the calculation with SMRS.

I. Observations

As a general observation, both LO and NLO CEM calculations provide a reasonable description of x_F distributions of J/ψ production in the energy range considered (Figs. 3–10). We note that the large difference in the magnitude between LO and NLO is compensated by the F factor. The F factors for the xFitter and JAM PDFs are relatively stable across the range of collision energies,

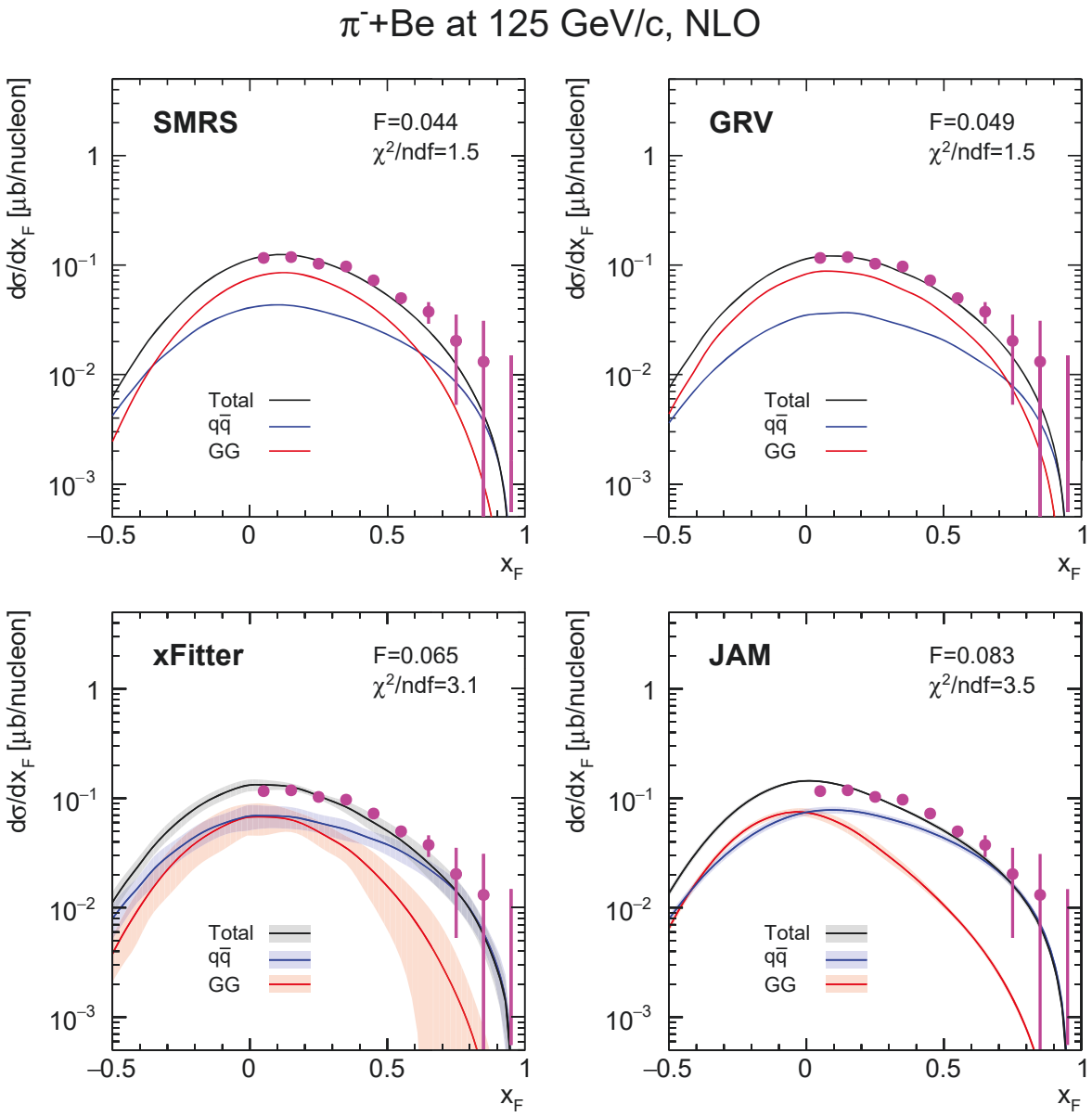

FIG. 9. Comparison of the NLO CEM results for the SMRS, GRV, xFitter, and JAM PDFs, with the $d\sigma/dx_F$ data of J/ψ production off the hydrogen target with a 125-GeV/c π^- beam from the E537 experiment [73]. The total cross sections and $q\bar{q}$ and GG contributions are denoted as black, blue, and red lines, respectively.

while the factors for SMRS and GRV PDFs show a mild rise toward low energies. From the comparison between data and calculations, interesting observations are summarized below.

(i) The importance of the GG contribution relative to that of $q\bar{q}$ is greatly enhanced in the NLO calculation. As for the description of the large-x_F data points for the pion beam larger than 125 GeV/c, the χ^2/ndf values with the NLO calculations generally improve for the results with

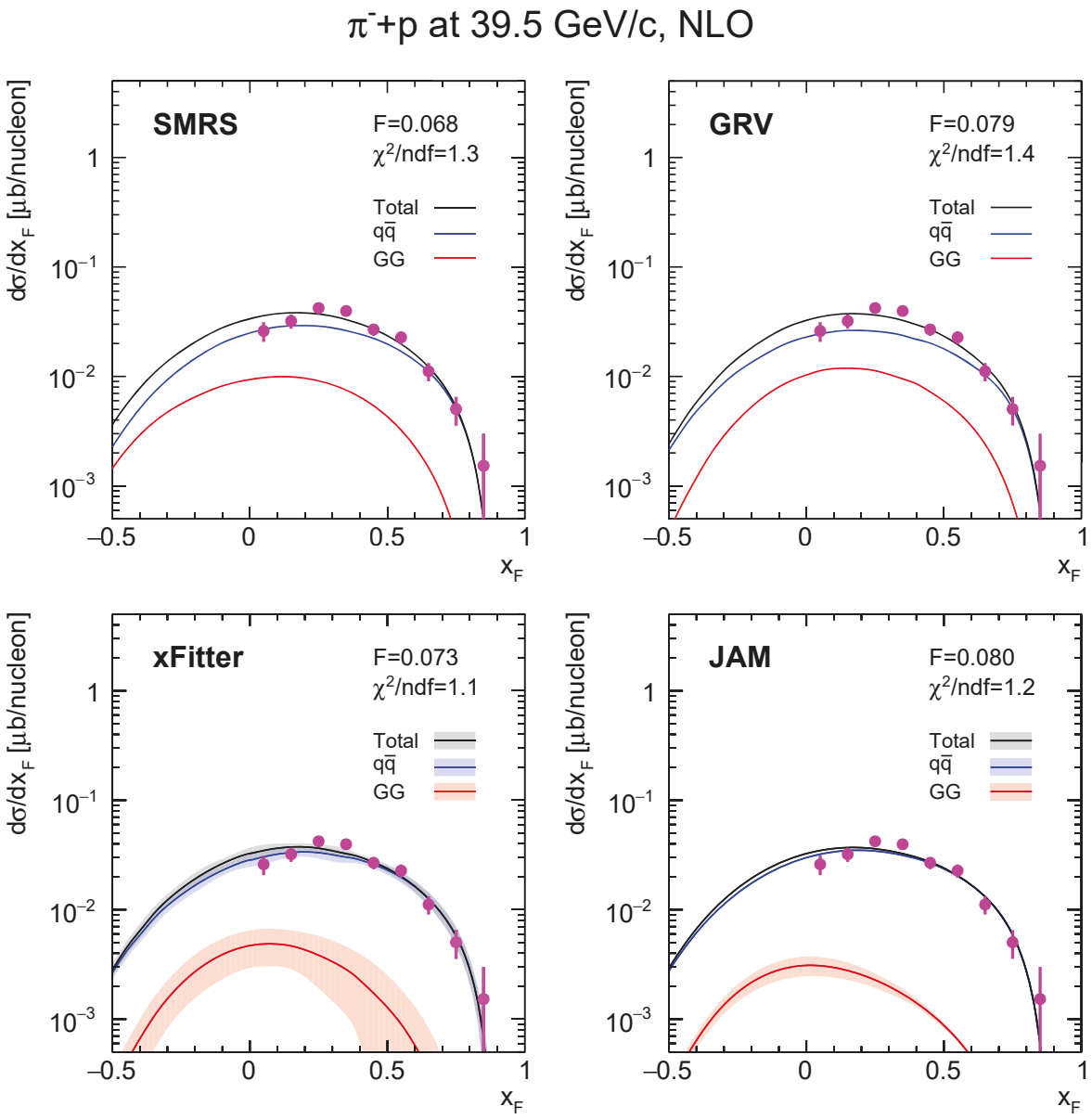

FIG. 10. Comparison of the NLO CEM results for the SMRS, GRV, xFitter, and JAM PDFs, with the $d\sigma/dx_F$ data of J/ψ production off the hydrogen target with a 39.5-GeV/c π^- beam from the WA39 experiment [74]. The total cross sections and $q\bar{q}$ and GG contributions are denoted as black, blue and red lines, respectively.

SMRS and GRV, whereas those with xFitter and JAM become worse, compared to the LO ones; for example, see Fig. 3.

(ii) At low energies, the GG contribution is relatively small, but it increases rapidly with the increase of energy. The fraction of GG component is maximized around $x_F = 0$, corresponding

to the gluon density of pions at x ∼0.1–0.2. As a result of the rapid drop of the pion's gluon density toward $x = 1$ shown in Fig. 1(c), the GG contribution decreases dramatically toward large x_F. In contrast, the $q\bar{q}$ contribution falls off slower at high x_F because of the relatively strong pion valence antiquark density at large x. Consequently, the $q\bar{q}$ contribution has a broader x_F distribution than that of the GG contribution and the relative importance of $q\bar{q}$ rises at the large-x_F region. As mentioned before, CEM dictates the relative weighting between $q\bar{q}$ and GG subprocesses by the convolution of pQCD calculation and parton densities, and the F factor cannot modify the shape of $d\sigma/dx_F$. Therefore, adequate shapes of $d\sigma/dx_F$ distributions of individual GG and $q\bar{q}$ contributions from CEM calculations are required to achieve a reasonable description of data points at $x_F > 0.5$. Since the partonic cross sections and nucleon PDFs are basically common in the calculations [Eq. (1)], the variation of results shall originate from the difference in the folded pion partonic densities. The calculations with SMRS and GRV pion PDFs agree with the data overall, while significantly large χ^2/ndf values are found in the description of data with a beam momentum greater than 125 GeV/c for both xFitter and JAM pion PDFs.

(iii) At low beam energies such as 39.5 GeV/c in Fig. 10, the $q\bar{q}$ process is the dominant mechanism of J/ψ production over the whole x_F region. The data are much less, if at all, sensitive to the variation of the GG contribution. Good χ^2/ndf values are obtained for all four pion PDFs.

V. SYSTEMATIC STUDY

Through the comparison of data with calculations over a broad energy range, we have two major findings: (i) The large-x_F distribution of J/ψ production is sensitive to the pion gluon density; (ii) the central values of gluon densities of the recently available JAM and xFitter fall off too rapidly at large x and fail to describe the x_F distributions of J/ψ data. Judging from the consistency of observation for the datasets with proton and nuclear targets, the unaccounted nuclear medium effects such as the energy loss effect are unlikely to change the conclusions.

The uncertainties provided by xFitter and JAM can have an impact on the χ^2 values of the fits. We perform a new fit where the PDF uncertainties are added as theoretical errors into the covariance matrix of measurements for the calculation of the χ^2 values. Table III lists the best-fit F factor and χ^2/ndf values for the four pion PDFs without PDF uncertainties, as shown in Figs. 3–10, and those with inclusion of PDF uncertainties for xFitter and JAM. As expected, the χ^2/ndf value of the fit for both xFitter and JAM improves after taking into account the PDF uncertainties.

The F factor remains basically unchanged. Because of the relatively large uncertainties assigned by xFitter, the improvement of χ^2/ndf is more pronounced for xFitter than JAM, even though these two pion PDFs have similar central values in their large-x gluon distributions.

Data	SMRS		GRV		xFitter				JAM			
Experiment (P_{beam})	F	χ^2/ndf	F	χ^2/ndf	F	F^*	χ^2/ndf	χ^2/ndf*	F	F^*	χ^2/ndf	χ^2/ndf*
E672, E706 (515)	0.040	1.2	0.040	2.2	0.063	0.063	6.8	4.7	0.081	0.081	18.9	18.5
E705 (300)	0.052	2.3	0.053	1.9	0.073	0.076	3.2	1.3	0.086	0.086	16.1	15.9
NA3 (280)	0.046	1.5	0.049	2.0	0.067	0.069	5.0	3.2	0.081	0.081	10.4	10.3
NA3 (200)	0.046	2.1	0.050	2.2	0.065	0.066	5.0	1.3	0.081	0.081	7.7	7.6
WA11 (190)	0.054	5.0	0.058	7.2	0.078	0.076	19.4	6.2	0.091	0.091	73.7	72.9
NA3 (150)	0.065	1.1	0.071	1.0	0.089	0.091	2.6	1.6	0.108	0.108	3.9	3.8
E537 (125)	0.044	1.5	0.049	1.5	0.065	0.065	3.1	1.4	0.083	0.083	3.5	3.5
WA39 (39.5)	0.068	1.3	0.079	1.4	0.073	0.072	1.1	0.8	0.080	0.080	1.2	1.2

TABLE III. Results of F factor and χ^2/ndf value of the best fit of the NLO CEM calculations for SMRS, GRV, xFitter, and JAM pion PDFs to the data listed in Table II. The F^* factor and χ^2/ndf* are the ones corresponding to the fit with inclusion of PDF uncertainties for xFitter and JAM.

To check the sensitivity of the CEM calculation to various QCD parameters and the choice of nuclear PDFs, we have performed a systematic study. Taking the convention of the charm quark mass in Refs. [49–51], we test the variations of results by setting m_c to be 1.2 GeV/c^2. The dependence on the renormalization scale μ_R is checked by varying at 0.5, 1.0, and 2.0 m_c [55]. We also make a different choice of nCTEQ15 [80] as the nuclear PDF in the calculations with GRV, JAM, and xFitter. Overall, the above observations remain qualitatively valid with respect to all these systematic variations.

Figures 11 and 12 show the systematic study of comparing the E672/E706 data and CEM NLO calculation with GRV and JAM pion PDFs with the variation of m_c and μ_R. In total there are six settings of parameters under investigation. Overall, the charm quark mass m_c plays a more visible role than the renormalization scale μ_R in the systematic effect. With a smaller charm quark mass m_c, the fractions of $q\bar{q}$ decrease while the fractions of GG increase. The hadronization factor F drops with the decrease of m_c, in accordance with a large phase space of $c\bar{c}$ production in Eq. (1). The variation of the renormalization scale μ_R shows a similar but much less significant trend.

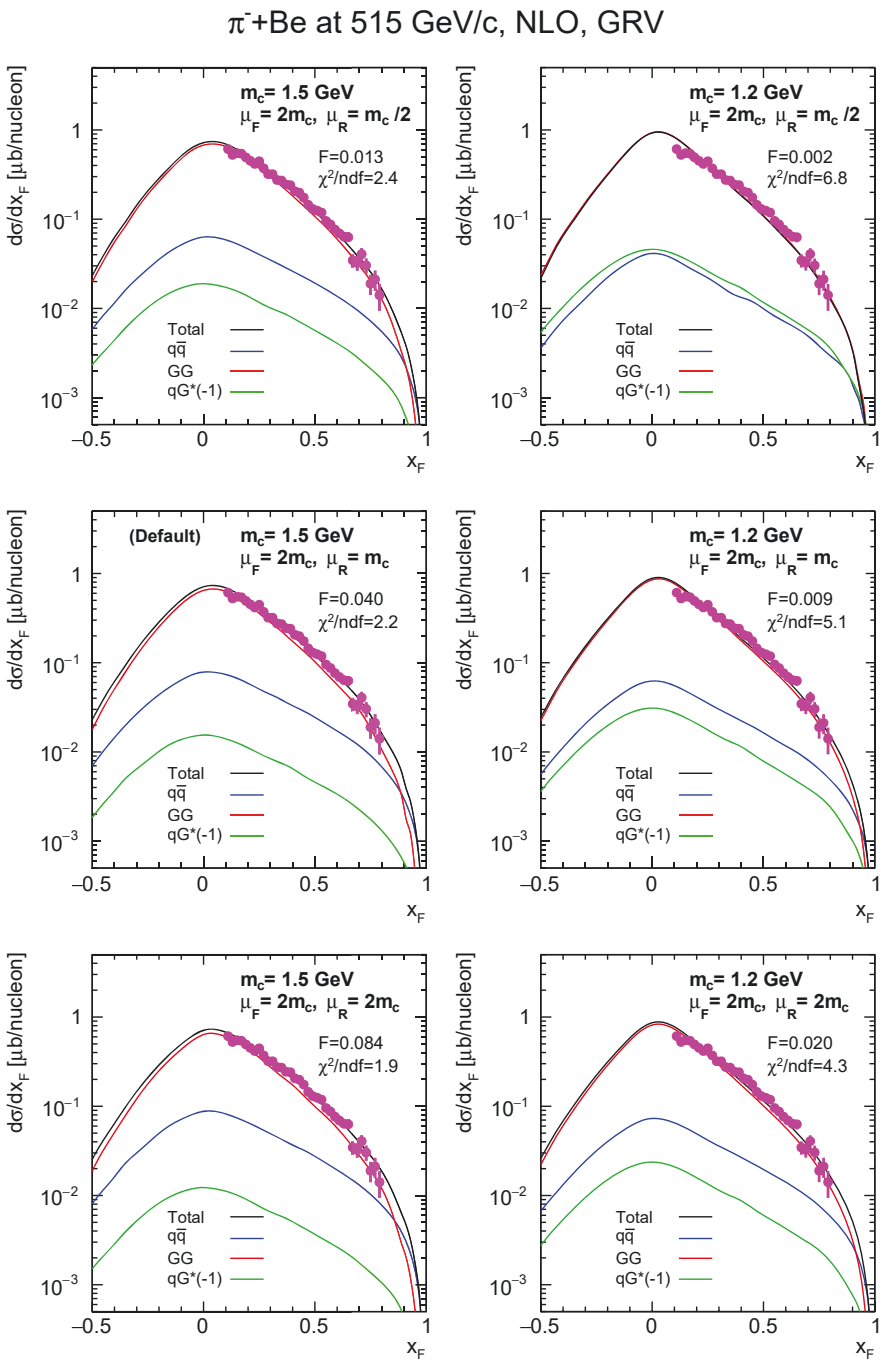

FIG. 11. The NLO CEM results with variation of charm quark mass m_c and renormalization scale μ_R, compared with the $d\sigma/dx_F$ data of J/ψ production off the beryllium target with a 515-GeV/c π^- beam from the E672/E706 experiment [68]. The pion PDFs used for the calculation is GRV. The total cross sections and $q\bar{q}$, GG, and $qG \times (-1)$ contributions are denoted as black, blue, red and green lines, respectively. The charm quark mass m_c, factorization scale μ_F, and renormalization scale μ_R used for the CEM calculation as well as the fit χ^2/ndf and F factors are displayed in each plot.

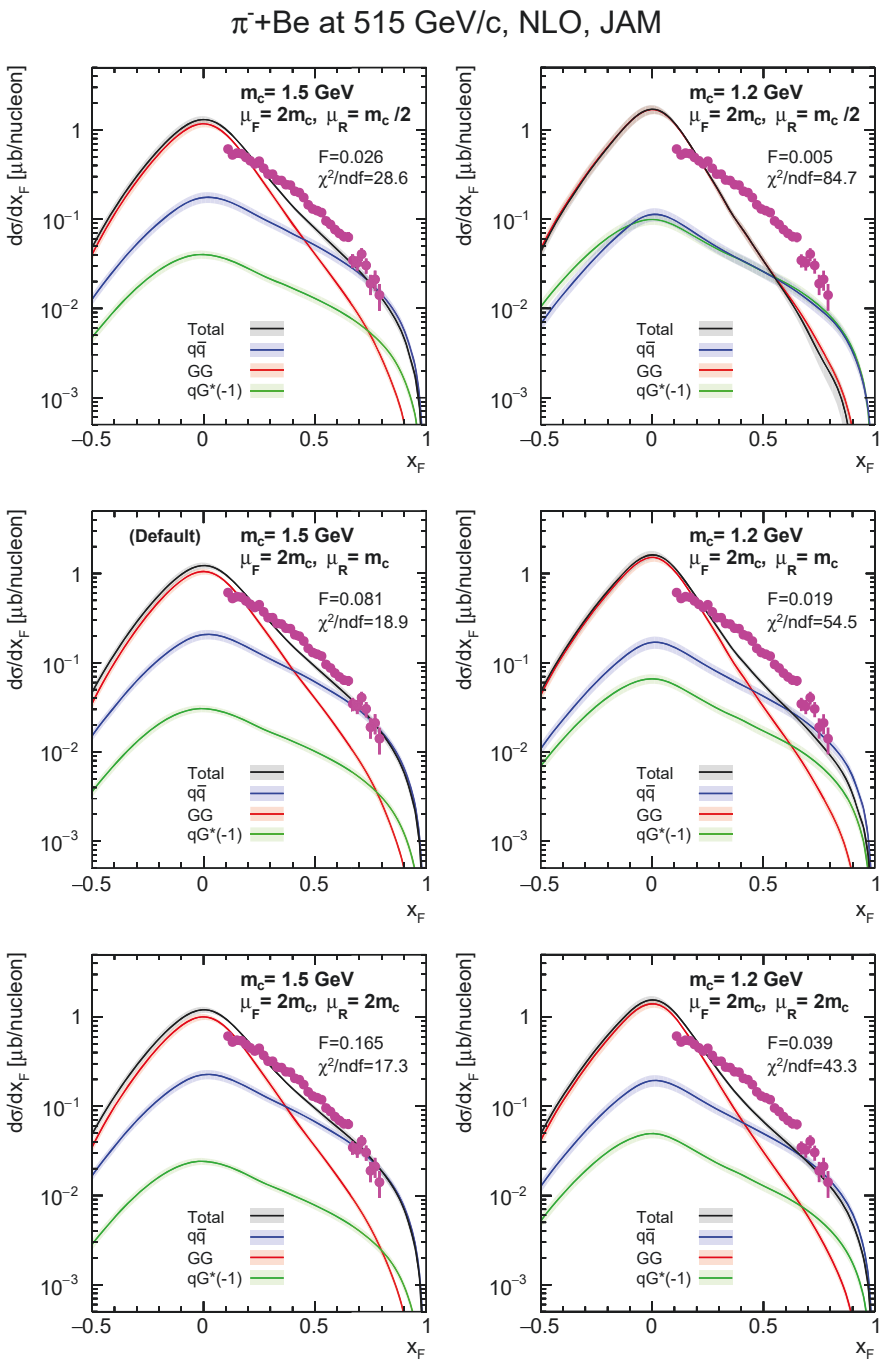

FIG. 12. The same as Fig. 11 but with the input of JAM pion PDFs.

For this dataset at the largest beam momentum of 515 GeV/c, the GG contribution is dominating in the CEM NLO calculation. A reduction of m_c from 1.5 to 1.2 GeV/c^2 reduces the relative contribution of $q\bar{q}$ and leads to a deterioration of χ^2/ndf for both GRV and JAM. Nevertheless, this effect is particularly significant in the case of JAM. With a reduction of the $q\bar{q}$ contribution,

the large-x gluon density of JAM PDFs is not strong enough to sustain enough GG contribution in accounting for the cross sections at large x_F. The information of F factor and χ^2/ndf for the systematic study of this dataset with the SMRS, GRV, xFitter, and JAM pion PDFs, is shown in Table IV.

Setting		F				χ^2/ndf			
m_c	$\frac{\mu_R}{m_c}$	SMRS	GRV	xFitter	JAM	SMRS	GRV	xFitter	JAM
1.2	0.5	0.002	0.002	0.004	0.004	3.2	6.8	20.8	75.0
1.2	1.0	0.010	0.009	0.014	0.017	2.1	5.0	12.7	50.6
1.2	2.0	0.020	0.020	0.030	0.035	1.7	4.3	9.8	40.8
1.5	0.5	0.013	0.013	0.019	0.024	1.4	2.4	7.2	28.4
1.5	1.0	0.040	0.040	0.059	0.075	1.1	2.1	5.5	19.9
1.5	2.0	0.084	0.084	0.121	0.153	1.0	1.9	4.1	17.6

TABLE IV. Results of F factor and χ^2/ndf value of the best fit of the CEM calculations for SMRS, GRV, xFitter and JAM pion PDFs to the data of J/ψ production off the beryllium target with a 515-GeV/c π^- beam [69], with the systematic variation of charm quark mass m_c between 1.2 and 1.5 GeV/c^2, and renormalization scale μ_R at 0.5, 1.0, and 2.0 m_c.

From the systematic study of all datasets, the NLO CEM results clearly favor SMRS and GRV, especially at high energies. The χ^2/ndf, representing the performance of data description, strongly correlates with how large the magnitude of gluon density is in the valence region. As shown in Fig. 1(c), SMRS and GRV have a significantly larger gluon density at large x than xFitter and JAM. Overall, our studies indicate that high-energy J/ψ data have an increased sensitivity to the pion large-x gluon density in the NLO calculations, resulting from the enhanced importance of the GG contribution. On the other hand, the relatively small difference in the valence-quark distributions for various PDFs plays a minor role in J/ψ production if away from the threshold region, as seen in the comparison of results of SMRS and GRV.

VI. DISCUSSION

From the early CEM LO studies [3, 4], it was known that the fixed-target J/ψ production is sensitive to pion valence-quark distribution at low energies via the $q\bar{q}$ mechanism and to the

GG contribution at high energies [3]. In this study, we confirm the sensitivity of the fixed-target J/ψ data to the pion's gluon density in the valence-quark region within the CEM. Moreover, we show that this sensitivity is further enhanced when the NLO calculations are performed. The hadronization factors F with the default parameter setting are found in the range of 0.04–0.08, consistent with the ones determined from the fixed-target proton-induced J/ψ data [49]. This finding supports the usage of the CEM approach to access the pion PDFs from J/ψ production.

The NLO CEM calculations suggest that the x_F distributions for fixed-target J/ψ production can serve as a tool for accessing the pion partonic densities. At low energies the data are predominantly sensitive to the pion's valence-quark distributions, while at high energies the data become increasingly sensitive to the gluon distributions in the pion. Thus, a global fit taking into account the J/ψ data across a broad energy range is expected to be helpful in pinning down the large-x gluon density of pions better. At low energies where the $q\bar{q}$ mechanism dominates, the pion-induced J/ψ production, having much larger cross sections than the Drell-Yan process, could be a powerful alternative to the Drell-Yan process in probing the quark distributions of pions.

We note that the recent effort to include leading neutron DIS data in the JAM global analysis has provided new constraints on the pion's sea and gluon distributions at $x \sim$0.001–0.1 [18]. Unfortunately, the existing leading neutron DIS data are not sensitive to the PDF at $x > 0.1$. It is also important to include the direct-photon production as well as J/ψ production data in the future global fits to place stringent constraints on the gluon distributions at large x. As shown in this study, the JAM gluon density at large x is too low to reproduce the J/ψ data. The upcoming tagged DIS experiment at the Jefferson Lab will be able to extend the sensitive region up to $x = 0.2$ [81].

VII. SUMMARY

We have examined the available pion PDFs extracted from the global fit to Drell-Yan, prompt-photon production or leading neutron DIS data. These PDFs present pronounced differences, particularly in the gluon distributions. We have calculated their total and x_F differential cross sections for pion-induced J/ψ production using the CEM framework at NLO. The calculations are compared to the data using hydrogen and light nuclear targets.

We observe the importance of the gluon fusion process in J/ψ production, especially at high (fixed-target) energies. We find that this dominance is even more pronounced in the NLO calculation. Since the calculated shapes of x_F distributions of GG and $q\bar{q}$ contributions are directly

related to the parton x distributions of corresponding PDFs, a proper description of J/ψ production data, especially for $x_F > 0.5$, imposes a strong constraint on the relevant pion's parton PDFs. Among the four pion PDFs examined, the CEM NLO calculations favor SMRS and GRV PDFs whose gluon densities at $x > 0.1$ are higher, compared with xFitter and JAM PDFs. The GG contribution from the latter two pion PDFs drops too fast toward $x_F = 1$ to describe the data.

Within the CEM, our study clearly indicates that the fixed-target pion-induced J/ψ data could be useful in constraining the pion gluon density, particularly at the large-x region. It will be interesting to perform similar studies using the more sophisticated NRQCD approach. In the near future, new measurements of Drell-Yan as well as J/ψ data in πA reactions will be available from the CERN COMPASS experiment. While further theoretical efforts are required to reduce the model dependence in describing the J/ψ production, we believe that it is important to include the existing large amount of pion-induced J/ψ data as well as the new ones in future pion global analysis.

ACKNOWLEDGMENTS

We thank Nobuo Sato and Ivan Novikov for providing us with LHAPDF6-compatible grid files of JAM and xFitter PDFs. This work was supported in part by the U.S. National Science Foundation and the Ministry of Science and Technology of Taiwan.

[1] H. Yukawa, Proc. Phys.-Math. Soc. Jpn.**17**, 48 (1935).

[2] T. Horn and C. D. Roberts, J. Phys. G **43**, 073001 (2016).

[3] M. Gluck, J. F. Owens, and E. Reya, Phys. Rev. D **17**, 2324 (1978).

[4] V. D. Barger, W. Y. Keung, and R. J. N. Phillips, Z. Phys. C **6**, 169 (1980).

[5] V. A. Khoze, A. D. Martin, and M. G. Ryskin, Eur. Phys. J. C **48**, 797 (2006).

[6] J. R. McKenney, N. Sato, W. Melnitchouk, and C. R. Ji, Phys. Rev. D **93**, 054011 (2016).

[7] S. X. Qin, C. Chen, C. Mezrag, and C. D. Roberts, Phys. Rev. C **97**, 015203 (2018)

[8] R. J. Perry, A. s. Kzlers, and A. W. Thomas, Phys. Rev. C **100**, 025206 (2019).

[9] J. T. Londergan, G. Q. Liu, E. N. Rodionov, and A. W. Thomas, Phys. Lett. B **361**, 110 (1995).

[10] B. Adams *et al.*, Letter of Intent: A New QCD facility at the M2 beam line of the CERN SPS (COMPASS++/AMBER), arXiv:808.00848; https://nqf-m2.web.cern.ch/.

[11] J. F. Owens, Phys. Rev. D **30**, 943 (1984).

[12] P. Aurenche, R. Baier, M. Fontannaz, M. N. Kienzle-Focacci, and M. Werlen, Phys. Lett. B **233**, 517 (1989).

[13] P. J. Sutton, A. D. Martin, R. G. Roberts, and W. J. Stirling, Phys. Rev. D **45**, 2349 (1992).

[14] M. Gluck, E. Reya, and A. Vogt, Z. Phys. C **53**, 651 (1992).

[15] M. Gluck, E. Reya, and I. Schienbein, Eur. Phys. J. C **10**, 313 (1999).

[16] C. Bourrely and J. Soffer, Nucl. Phys. **A981**, 118 (2019).

[17] I. Novikov *et al.*, Phys. Rev. D **102**, 014040 (2020).

[18] P. C. Barry, N. Sato, W. Melnitchouk, and C. R. Ji, Phys. Rev. Lett. **121**,152001 (2018).

[19] M. Aghasyan *et al.* (COMPASS Collaboration), Phys. Rev. Lett. **119**, 112002 (2017); C. Y. Hsieh, JPS Conf. Proc. **26**, 031003 (2019).

[20] A. Accardi *et al.*, Eur. Phys. J. A **52**, 268 (2016).

[21] A. C. Aguilar *et al.*, Eur. Phys. J. A **55**, 190 (2019).

[22] S. i. Nam, Phys. Rev. D **86**, 074005 (2012).

[23] A. Watanabe, C. W. Kao, and K. Suzuki, Phys. Rev. D **94**, 114008 (2016).

[24] A. Watanabe, T. Sawada, and C. W. Kao, Phys. Rev. D **97**, 074015 (2018).

[25] P. T. P. Hutauruk, I. C. Cloet and A. W. Thomas, Phys. Rev. C **94**, 035201 (2016).

[26] J. Lan, C. Mondal, S. Jia, X. Zhao, and J. P. Vary, Phys. Rev. Lett. **122**, 172001 (2019).

[27] J. Lan, C. Mondal, S. Jia, X. Zhao, and J. P. Vary, Phys. Rev. D **101**, 034024 (2020).

[28] G. F. de Teramond *et al.* (HLFHS Collaboration), Phys. Rev. Lett. **120**, 182001 (2018).

[29] A. Watanabe, T. Sawada, and M. Huang, Phys. Lett. B **805**, 135470 (2020).

[30] C. Han, H. Xing, X. Wang, Q. Fu, R. Wang, and X. Chen, Phys. Lett. B **800**, 135066 (2020).

[31] L. Chang, C. Mezrag, H. Moutarde, C. D. Roberts, J. Rodrguez-Quintero, and P. C. Tandy, Phys. Lett. B **737**, 23 (2014).

[32] L. Chang and A. W. Thomas, Phys. Lett. B **749**, 547 (2015).

[33] C. Chen, L. Chang, C. D. Roberts, S. Wan, and H. S. Zong, Phys. Rev. D **93**, 074021 (2016).

[34] C. Shi, C. Mezrag, and H. s. Zong, Phys. Rev. D **98**, 054029 (2018).

[35] K. D. Bednar, I. C. Clot, and P. C. Tandy, Phys. Rev. Lett. **124**, 042002 (2020).

[36] M. Ding, K. Raya, D. Binosi, L. Chang, C. D. Roberts, and S. M. Schmidt, Phys. Rev. D **101**, 054014 (2020).

[37] X. Ji, Phys. Rev. Lett. **110**, 262002 (2013); X. Ji, Y. S. Liu, Y. Liu, J. H. Zhang, and Y. Zhao, arXiv:2004.03543.

[38] J. H. Zhang, J. W. Chen, L. Jin, H. W. Lin, A. Schfer, and Y. Zhao, Phys. Rev. D **100**, 034505 (2019).

[39] R. S. Sufian, J. Karpie, C. Egerer, K. Orginos, J. W. Qiu, and D. G. Richards, Phys. Rev. D **99**, 074507 (2019).

[40] T. Izubuchi, L. Jin, C. Kallidonis, N. Karthik, S. Mukherjee, P. Petreczky, C. Shugert, and S. Syritsyn, Phys. Rev. D **100**, 034516 (2019).

[41] B. Jo, J. Karpie, K. Orginos, A. V. Radyushkin, D. G. Richards, R. S. Sufian, and S. Zafeiropoulos, Phys. Rev. D **100**, 114512 (2019).

[42] R. S. Sufian *et al.*, arXiv:2001.04960.

[43] M. B. Einhorn and S. D. Ellis, Phys. Rev. D **12**, 2007 (1975); H. Fritzsch, Phys. Lett. **67B**, 217 (1977); F. Halzen, Phys. Lett. **69B**, 105 (1977).

[44] C. H. Chang, Nucl. Phys. **B172**, 425 (1980); E. L. Berger and D. L. Jones, Phys. Rev. D **23**, 1521 (1981); R. Baier and R. Ruckl, Phys. Lett. **102B**, 364 (1981), Z. Phys. C **19**, 251 (1983).

[45] G. T. Bodwin, E. Braaten, and G. P. Lepage, Phys. Rev. D **51**, 1125 (1995); **55**, 5853(E) (1997).

[46] G. A. Schuler, arXiv:hep-ph/9403387; Z. Phys. C **71**, 317 (1996); N. Brambilla *et al.*, Eur. Phys. J. C **71**, 1534 (2011); A. Andronic *et al.*, Eur. Phys. J. C **76**, 107 (2016); J. P. Lansberg, arXiv:1903.09185.

[47] F. Maltoni *et al.*, Phys. Lett. B **638**, 202 (2006).

[48] G. T. Bodwin, E. Braaten, and J. Lee, Phys. Rev. D **72**, 014004 (2005).

[49] R. Gavai, D. Kharzeev, H. Satz, G. A. Schuler, K. Sridhar, and R. Vogt, Int. J. Mod. Phys. A **10**, 3043 (1995).

[50] G. A. Schuler and R. Vogt, Phys. Lett. B **387**, 181 (1996).

[51] R. E. Nelson, R. Vogt, and A. D. Frawley, Phys. Rev. C **87**, 014908 (2013).

[52] J. P. Lansberg, H. S. Shao, N. Yamanaka, Y. J. Zhang, and C. Nos, Phys. Lett. B **807**, 135559 (2020).

[53] P. Nason, S. Dawson, and R. K. Ellis, Nucl. Phys. **B303**, 607 (1988).

[54] P. Nason, S. Dawson, and R. K. Ellis, Nucl. Phys. **B327**, 49 (1989); **B335**, 260(E) (1990).

[55] M. L. Mangano, P. Nason, and G. Ridolfi, Nucl. Phys. **B405**, 507 (1993).

[56] J. Badier *et al.* (NA3 Collaboration), Z. Phys. C **18**, 281 (1983).

[57] E. Anassontzis *et al.*, Phys. Rev. D **38**, 1377 (1988).

[58] S. Falciano *et al.* (NA10 Collaboration), Z. Phys. C **31**, 513 (1986); M. Guanziroli *et al.*, Z. Phys. C **37**, 545 (1988).

[59] J. S. Conway *et al.* (E615 Collaboration), Phys. Rev. D **39**, 92 (1989); J. G. Heinrich *et al.*, Phys. Rev. D **44**, 1909 (1991).

[60] M. Bonesini *et al.* (WA70 Collaboration), Z. Phys. C **37**, 535 (1988).

[61] S. Chekanov *et al.* (ZEUS Collaboration), Nucl. Phys. **B637**, 3 (2002).

[62] F. D. Aaron *et al.* (H1 Collaboration), Eur. Phys. J. C **68**, 381 (2010).

[63] M. Aicher, A. Schafer, and W. Vogelsang, Phys. Rev. Lett. **105**, 252003 (2010).

[64] S. Dulat *et al.*, Phys. Rev. D **93**, 033006 (2016).

[65] M. R. Whalley, D. Bourilkov and R. C. Group, arXiv:hep-ph/0508110; `https://lhapdf.hepforge.org/lhapdf5/`.

[66] A. Buckley, J. Ferrando, S. Lloyd, K. Nordstrm, B. Page, M. Rfenacht, M. Schnherr and G. Watt, Eur. Phys. J. C **75**, 132 (2015); `https://lhapdf.hepforge.org/`.

[67] Y. Alexandrov *et al.* (BEATRICE Collaboration), Nucl. Phys. **B557**, 3 (1999).

[68] A. Gribushin *et al.* (E672 and E706 Collaborations), Phys. Rev. D **53**, 4723 (1996).

[69] L. Antoniazzi *et al.* (E705 Collaboration), Phys. Rev. D **46**, 4828 (1992).

[70] J. Badier *et al.* (NA3 Collaboration), Z. Phys. C **20**, 101 (1983).

[71] J. G. Branson *et al.*, Phys. Rev. Lett. **38**, 1331 (1977).

[72] J. G. McEwen *et al.*, Phys. Lett. **121B**, 198 (1983).

[73] S. Tzamarias *et al.*, Phys. Rev. D **48**, 5067 (1993).

[74] M. J. Corden *et al.*, Phys. Lett. **98B**, 220 (1981).

[75] J. LeBritton *et al.*, Phys. Lett. **81B**, 401 (1979).

[76] Y. B. Bushnin *et al.*, Phys. Lett. **72B**, 269 (1977).

[77] M. J. Corden *et al.*, Phys. Lett. **96B**, 411 (1980).

[78] K. J. Eskola, P. Paakkinen, H. Paukkunen, and C. A. Salgado, Eur. Phys. J. C **77**, 163 (2017).

[79] P. Charpentier, Ph.D. thesis, Université de Paris-Sud, 1983.

[80] K. Kovarik *et al.*, Phys. Rev. D **93**, 085037 (2016).

[81] Jefferson Lab experiment PR12-15-006, Measurement of Tagged Deep-Inelastic Scattering (TDIS), `https://www.jlab.org/exp_prog/proposals/14/PR12-14-010.pdf`.